ISSN 1063-7729, Astronomy Reports, 2016, Vol. 60, No. 2, pp. 211–219. © Pleiades Publishing, Ltd., 2016.
Original Russian Text © A.G. Rudnitskii, R. Karuppusamy, M.V. Popov, V.A. Soglasnov, 2016, published in Astronomicheskii Zhurnal, 2016, Vol. 93, No. 2, pp. 167–176.

Studies of Cosmic Plasma using RadioAstron VLBI Observations of Giant Pulses of the Pulsar B0531+21

A. G. Rudnitskii[1*], R. Karuppusamy[2], M. V. Popov[1***], and V. A. Soglasnov[1****]**

[1] *Astro Space Center, Lebedev Physical Institute, Russian Academy of Sciences, Profsoyuznaya ul. 84/32, Moscow, 117997 Russia*

[2] *Max Planck Institute for Radio Astronomy, Auf dem Hügel 69, D-53121 Bonn, Germany*

Received May 14, 2015; in final form, September 4, 2015

Abstract—The structure of the interstellar plasma in the direction of the pulsar in the Crab Nebula is studied using several sets of space-VLBI observations obtained with networks of ground telescopes and the RadioAstron space antenna at 18 and 92 cm. Six observing sessions spanning two years are analyzed. Giant pulses are used to probe the cosmic plasma, making it possible to measure the scattering parameters without averaging. More than 4000 giant pulses were detected. The interferometer responses (visibility functions) on ground and ground–space baselines are analyzed. On the ground baselines, the visibility function as a function of delay is dominated by a narrow feature at zero delay with a width of $\delta\tau \approx 1/B$, where B is the receiver bandwidth. This is typical for compact continuum sources. On the ground–space baselines, the visibility function contains a set of features superposed on each other and distributed within a certain interval of delays, which we identify with the scattering time for the interfering rays τ. The amplitude of the visibility function on ground baselines falls with increasing baseline; the scattering disk is partially resolved at 18 cm and fully resolved at 92 cm. Estimates of the scattering angle θ give 0.5–1.3 mas at 18 cm and 14.0 mas at 92 cm. The measured values of θ and τ are compared to estimate the distance from the source to the effective scattering screen, which is found at various epochs to be located at distances from 0.33 to 0.96 of the distance from the observer to the pulsar, about 2 kpc. The screen is close to the Crab Nebula at epochs of strong scattering, confirming that scattering on inhomogeneities in the plasma in the vicinity of the nebula itself dominates at these epochs.

DOI: 10.1134/S1063772916020116

1. INTRODUCTION

The interstellar medium contains free electrons that are non-uniformly distributed in space. These electron-density inhomogeneities have a wide range of scales, from several kilometers to hundreds of AU. Small-scale inhomogeneities refract radio waves, causing them to travel along a variety of paths. The interference of multiple rays coming from a spatially coherent source forms a random diffraction pattern near the Earth, with a characteristic frequency scale $\Delta\nu = 1/2\pi\tau$, where τ is the typical delay of the rays. Pulsars are compact sources providing a high level of coherence for the different propagation paths. Their high proper motions (transverse velocities) mean that the interference pattern changes appreciably on characteristic times $\Delta t = \lambda/\theta V$ from minutes to hours, where λ is the wavelength, θ the angle by which the rays from the source are scattered, and V the mean-weighted observed velocity of the pulsar relative to the medium.

A whole series of effects are observed in this connection, which were considered by Scheuer [1] soon after the discovery of pulsars, and subsequently analyzed theoretically by Rickett [2]. Observable effects of scattering include scintillation (modulation of the intensity of the pulses), an increase in the source angular size θ with decreasing frequency, and an increase in the pulse duration τ. The origin of the variation of the angular size as a result of scattering is the propagation of the radiation to the observer along multiple paths, which causes a compact, point-like source to appear extended. Phenomena due to scattering of the radio emission of pulsars in the interstellar medium can be used to study the structure of small-scale electron-density fluctuations on scales from at least 1000 km to 10 AU. Large-scale inhomogeneities of the ionized component of the interstellar medium give rise to refractive effects, manifest as slow variations of the flux density and angular shifts

*E-mail: almax1024@gmail.com
**E-mail: ramesh@mpifr-bonn.mpg.de
***E-mail: mwpopov@gmail.com
****E-mail: vsoglasn@asc.rssi.ru

of the apparent source position. Analyzing observations of diffractive and refractive scintillations together with variations in the dispersion measure and rotation measure, Shishov et al. [3, 4] showed that the spectrum of the inhomogeneities is a Kolmogorov spectrum with index $-11/3$ over a wide range of spatial scales.

However, deviations from a Kolmogorov spectrum have been found in some directions and for a number of pulsars [5–7]. The shape of the inhomogeneity spectrum was studied by Shishov [8]. Pulsars are the main source of our information about the structure of inhomogeneities in the interstellar plasma. Despite many years of studies, we do not yet have a full understanding of the origin, development, and dissipation of turbulence in the interstellar medium. There are likewise no definitive answers to the question of what phase of the interstellar medium is mainly responsible for the observed scintillation, how matter is distributed along the line of sight, or what is the relationship between random turbulence and deterministic structures. Thus, studying the effects of scattering using observations of pulsar radio pulses remains a relevant modern problem. The use of the giant pulses (GPs) emitted by some pulsars is of special interest. The most promising target of this type is the Crab Nebula pulsar, B0531+21.

B0531+21 is a relatively young pulsar. It is located in the Crab Nebula—the supernova remnant SN1054, at a distance of about 2 kpc from the Sun. The pulse profile includes the main pulse and an interpulse. GPs are detected at the rotational phases of the main pulse and interpulse. The properties of the GPs of this pulsar have been well studied [9–11]. The integrated spectral energy distribution of the GPs follows a power law with indices from -1.7 to -3.2, and the highest values of the peak flux densities reach millions of Jy. A distinguishing property of this pulsar is that its profile is formed fully of giant pulses [12].

The GPs from the Crab pulsar provide an excellent tool for probing the interstellar plasma, since they can be used to measure numerous scattering parameters without the need to carry out averaging. Very Long Baseline Interferometry (VLBI) observations of the Crab pulsar GPs were carried out earlier at 2.3 GHz using the Kalyazin and Algonquin radio telescopes [13]. This pulsar has been observed more recently as part of the RadioAstron project [14]. The first results for RadioAstron studies of pulsars were published by Smirnova et al. [7]. Here, we analyze the shape of the amplitude of the visibility function for ground and ground–space VLBI baselines for sessions carried out from 2011 through 2013. We have measured the angular size of the scattering disk θ and the scattering time scale τ, and used these measurements to estimate the location of the effective scattering screen along the line of sight.

2. OBSERVATIONS

The scientific program of the RadioAstron mission was divided into several atages. The first was comprised of the RadioAstron Fringe Search (RAFS) program, for which observations were carried out at the end of 2011 and beginning of 2012. This was followed by the RadioAstron Early Science (RAES) program, which continued to the middle of 2013, and the RadioAstron Key Science (RAKS) program, which has run since 2013 based on a yearly call for scientific proposals (Announcements of Opportunity: AO-1, AO-2, AO-3).

From 2011 through 2013, six sets of VLBI observations of the Crab pulsar were carried out using the RadioAstron space radio telescope. The main characteristics of these observing sessions are given in Table 1. Radio telescopes of the European and global VLBI networks acted as ground stations for the observations. Four sessions were carried out at 18 cm and one at 92 cm; one session was conducted as part of the RAFS program, three as part of the RAES program, and two as part of the RAKS program. The standard frequency scheme for the RadioAstron project, with the frequencies recorded in two circular-polarization channels, was used: upper and lower sidebands with a width of 16 MHz were recorded at 18 cm, while only the upper sideband was recorded at 92 cm. A single-digit digitization of the signal (clipping) was carried out onboard the spacecraft, and the ground telescopes applied two-bit digitization.

3. DATA REDUCTION

The preliminary reduction of the data was conducted on the correlator of the Astro Space Center (ASC) [15]. A regime for pulsars applying incoherent dedispersion lay at the basis of the reduction procedure. An algorithm designed to search for and correlate the GPs was developed. The essence of this algorithm is to obtain the cross-correlation function via an inverse Fourier transform of the complex cross-spectrum for each elementary data sample (1024 points), then estimate the amplitude of the interferometric response using a specified criterion.

Initially, an 8σ criterion was used when searching for the GPs, where σ represents the rms fluctuations of the cross-correlation function for a noise signal that does not contain any pulses. This criterion is guaranteed to filter out false detections. However, this criterion was lowered to 6σ in the subsequent analysis, making it possible to improve the data statistics

Table 1. List of observing sessions of the Crab pulsar carried out as part of the scientific program of the RadioAstron mission

Session	Date	Observing time	B (km)	λ (cm); ν (MHz)	Ground telescopes	Correlations
RAFS01	14.11.2011	23:00–00:00	46 000	18 (1660)	4	Ground–space baselines
RAES04A	02.03.2012	13:00–17:00	145 000	18 (1660)	8	Only ground baselines
RAES04B	06.03.2012	14:30–17:30	128 000	18 (1660)	8	Ground–space baselines
RAES04D	23.10.2012	07:00–09:00	113 000	18 (1660)	7	Ground–space baselines
RAKS02AD	27.10.2013	06:00–09:00	150 000	18 (1660)	4	Ground–space baselines
RAKS02AE	02.11.2013	19:30–08:40	40 000–57 000	92 (316)	5	Only ground baselines

by a factor of three, by increasing the number of detections of relatively weak GPs. In this latter case, the number of false detections was much less than 1%, and corresponded to about one to two false pulses per 1000 successful detections.

Additional analysis of possible false detections was carried out by checking the rotational phase of the detected pulses. The GPs of the Crab pulsar are known to occur only at the rotational phases of the main pulse and interpulse. We accordingly considered pulses whose rotational phases did not correspond with these values to be false detections.

The correlation was carried out using 1024 spectral channels and an integration time of 0.033 s. The number of spectral channels was chosen taking into consideration the fact that, due to our imperfect knowledge of the spacecraft orbit, the residual delay could reach 10 or more μs: 1024 channels, which corresponds to delays from -32 to 32 μs, covers the full range of possible residual delays, ruling out a lack of detections on the ground–space baselines due to inaccurate knowledge of the spacecraft orbit.

For the correlation function of the noise signal, the rms fluctuations σ should be equal to $1/\sqrt{n}$, where n is the number of data points in the analyzed signal. In our cases, $n = 1024$ (the number of spectral channels), and σ should be 0.03, making the detection limit of 6σ equal to 0.18.

The integration time was chosen to be roughly equal to the pular period for convenience in the operation of the GP search algorithm, which includes an incoherent dedispersion regime. In this regime, the chosen time interval, $\delta t_{\rm sol} = 0.033$ s, is divided into N intervals, each of which corresponds to a particular rotational phase in the pulsar period. Thus, the desired time resolution for the GP search was $\delta t = \delta t_{\rm sol}/N = 0.00011$ s, where the number of intervals was $N = 300$.

The ephemeris of the pulsar from the ATNF catalog [16][1] was used for the correlation, as well as the Jodrell Bank catalog [17].[2] We used the TEMPO2 software package to determine the longitudes of the GPs [18].

Since the correlated amplitudes for the individual GPs depend on their intensity, obtaining the correct dependence of the visibility-function amplitude on the projected baseline requires normalization to the correlated amplitude:

$$A_{norm} = \frac{A_{\rm corr}}{R}, \qquad (1)$$

where R is the normalization coefficient and $A_{\rm corr}$ is the initial, unnormalized value of the correlated amplitude.

In the general case,

$$R = \sqrt{\left(\sigma^2_{\rm 1tot} - \sigma^2_{\rm 1off}\right)\left(\sigma^2_{\rm 2tot} - \sigma^2_{\rm 2off}\right)}, \qquad (2)$$

where the subscripts 1 and 2 correspond to the two ground telescopes in a baseline, and $\sigma^2_{\rm tot}$ and $\sigma^2_{\rm off}$ are formally defined to be the amplitudes of the visibility function obtained from the autocorrelation spectra for windows on and off the pulse, respectively.

A different normalization relation was used for the ground–space baselines. The reason is that the growth of the signal relative to the noise, $\sigma^2_{\rm tot} - \sigma^2_{\rm off}$, can be very low, or even negative, for the space telescope, whose sensitivity is substantially lower than the sensitivity of the ground stations. Therefore, we applied the relation

$$R = \left(\sigma^2_{\rm 2tot} - \sigma^2_{\rm 2off}\right)\frac{\sigma_{\rm 1off}}{\sigma_{\rm 2off}}\sqrt{\frac{SEFD_2}{SEFD_1}}, \qquad (3)$$

where the subscript 1 corresponds to the space radio telescope and the subscript 2 to the ground telescope in the baseline. The known relationships between the effective noise temperatures of the telescopes (the system equivalent flux densities, SEFD) are used in this expression [19].

[1] http://www.atnf.csiro.au/people/pulsar/psrcat/

[2] http://www.jb.man.ac.uk/∼pulsar/crab.html

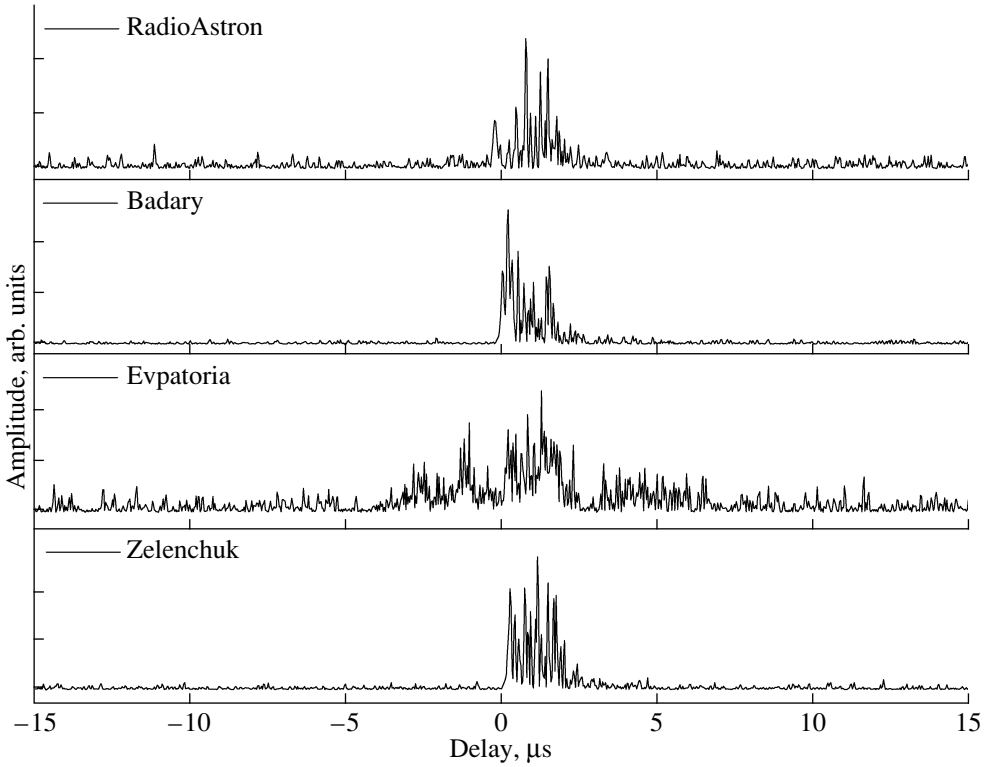

Fig. 1. Profile of the strongest giant pulse recorded in the session of November 14, 2011 (RAFS01) at $\lambda = 18$ cm, for the the RadioAstron space telescope and the Badary, Evpatoria, and Zelenchuk ground telescopes. Strong radio interference is present in the GP profile for the Evpatoria radio telescope.

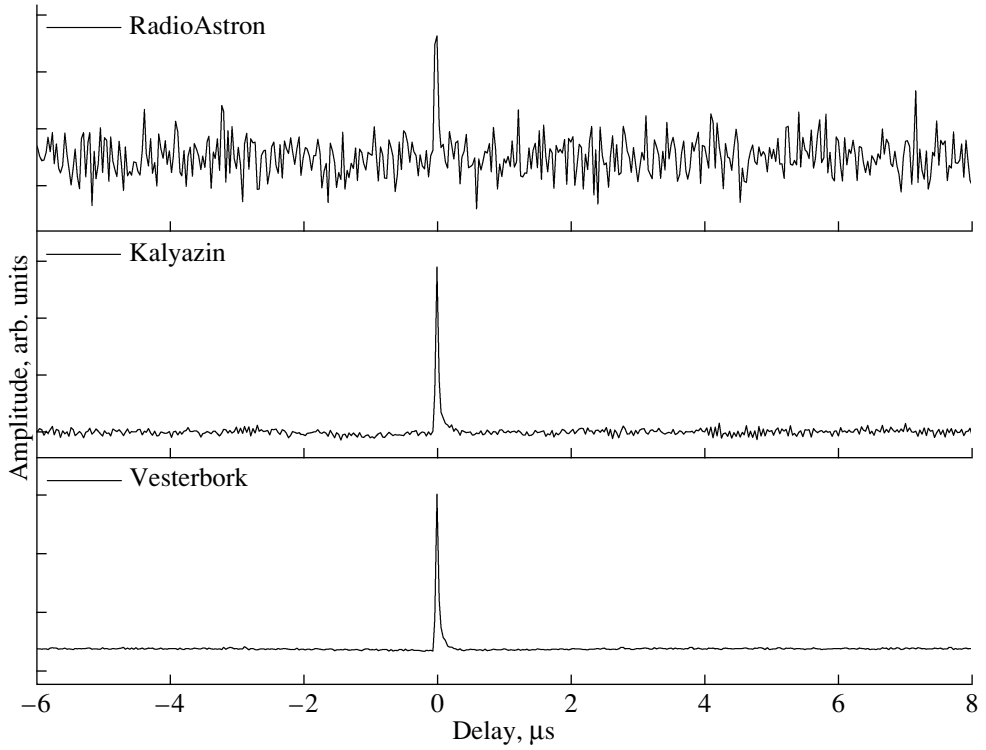

Fig. 2. Profile of one of the strongest giant pulses recorded in the session of November 2, 2013 (RAKS02AE) at $\lambda = 92$ cm, for the RadioAstron space telescope and the Kalyazin and Westerbork ground telescopes.

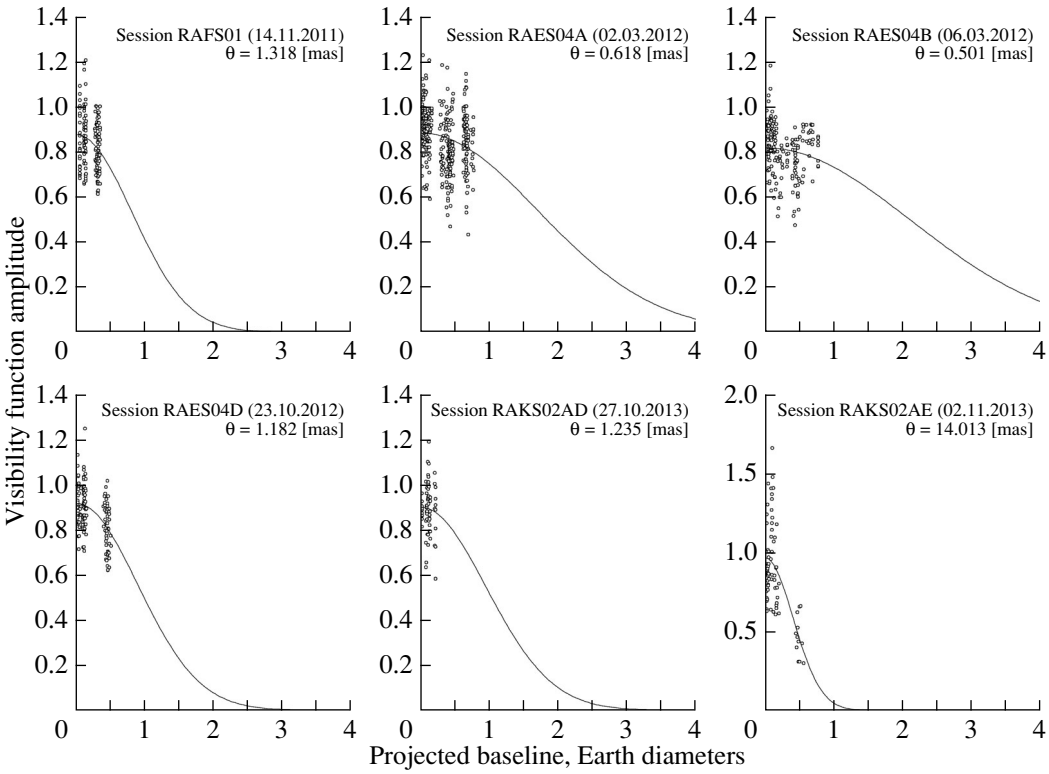

Fig. 3. Dependence of the maximum visibility amplitude on the projected baseline for all GPs and for all baselines. The projected baselines are indicated in Earth diameters. The sessions took place on November 14, 2011, March 2, 2012, March 6, 2012, October 23, 2012, October 27, 2013, and November 2, 2013 (from left to right and top to bottom).

4. ESTIMATES OF THE SCATTERING PARAMETERS

The cross-correlation function obtained after taking an inverse Fourier transform is the dependence of the amplitude of the visibility function on the time delay. Below, we use the term "visibility amplitude" in this context.

Figures 1 and 2 present profiles of individual GPs observed at 18 cm and 92 cm, respectively. Correlations on ground–space baselines were detected for four sessions at λ=18 cm. No detections were found on the ground–space baselines at λ=92 cm, in spite of the detection of GPs at the space radio telescope during its operation as a single antenna. We estimated the parameters of the scattering of the radio emission from the Crab pulsar using a model with a single thin screen [20].

The angular size of the scattering disk can be determined from the dependence of the visibility amplitude on the projected baseline. Adopting a model with a uniform scattering disk, this dependence can be approximated by the Gaussian distribution [21]

$$V(B) = V_0 \cdot e^{\left[-\frac{1}{2}\left(\frac{\pi}{\sqrt{2\ln 2}}\frac{\theta B}{\lambda}\right)^2\right]}, \qquad (4)$$

where θ is the angular size of the scattering disk in arcsec (full width at half-maximum level), B is the projected baseline in cm, and λ is the observing wavelength in cm.

The angular size of the scattering disk θ was determined by fitting the above expression to the distribution of the visibility amplitude as a function of the projected baseline. The uncertainty in the angular size was taken to be equal to the formal errors obtained from the least-squares fit of the distribution using (4). Figure 3 shows the dependences of the maximum visibility amplitude on the projected baseline. The dependences for all the GPs, for all combinations of baselines, and for each of the analyzed sessions are indicated. The solid curves show the fits of these dependences using (4).

As can be seen in Fig. 4, the shape of the visibility amplitude varies strongly in the transition from the ground to the ground–space baselines. The visibility amplitudes for the ground baselines (Fig. 4, right) have two features: one central and compact and the other no less intense but broad; the visibility amplitudes for the ground–space baselines (Fig. 4, left) display substantially different shapes, with numerous features. The shape of the visibility amplitude for the

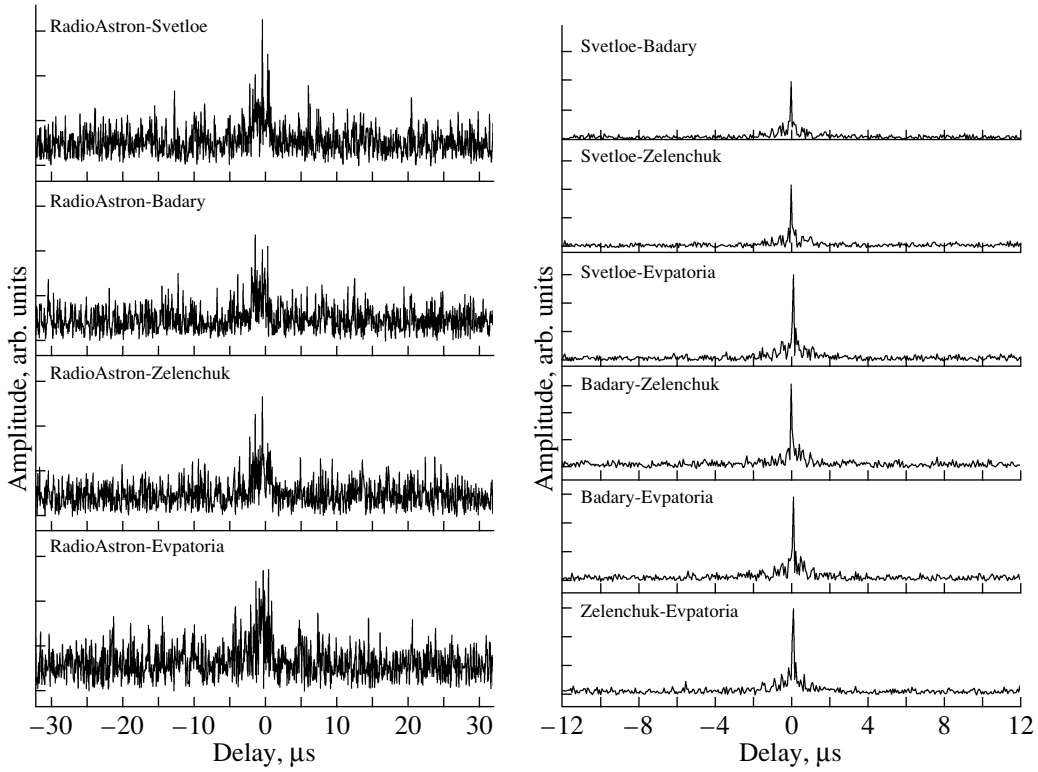

Fig. 4. Shape of the cross-correlation function for the giant pulse of 23 : 21 : 03.74, session RAFS01 (November 14, 2011), $\lambda = 18$ cm, for the ground–space baselines (left) and ground baselines (right).

ground–space baselines reflects the value of the time scale τ on which the scattering occurred.

Thus, the scattering time scale can be estimated using direct measurements on the ground–space baselines, by obtaining an exponential fit of the averaged visibility function, which corresponds to the broadened pulse shape [22, 23]. This was done when interferometer fringes were detected on the ground–space baselines. The uncertainty in the scattering time scale was taken to be the formal error obtained from the least-squares fit of the averaged visibility function,

$$A = C + A_0 \cdot e^{-x/\tau}, \tag{5}$$

where τ is the desired scattering time sale in microseconds.

Figure 5 depicts the mean visibility amplitudes for the four sessions in which interference fringes were detected on the ground–space baselines. We estimated the scattering time scales for these sessions using the above method. Such distortions of the visibility amplitude arise as the projected baseline increases when the baseline becomes larger than the radius of the diffraction spot.

The radius of the diffraction spot $R_{\rm diff}$ depends on the angular size of the scattering disk and the observing wavelength, and is related to these parameters as [24]

$$R_{\rm diff} = \sqrt{2\ln 2}\frac{\lambda}{\theta\pi}. \tag{6}$$

As can be seen in Table 1, the maximum projected ground–space baseline in the sessions exceeds the calculated size of the diffraction spots.

The character of the scintillations depends on the observing frequency. This dependence is characterized by the variation of the decorrelation bandwidth $\Delta\nu$ with frequency.

We determined the decorrelation bandwidth by analyzing the cross-correlation function of the mean auto-correlation spectra for two selected ground stations. The decorrelation bandwidth was estimated by obtaining an exponential fit of the cross-correlation function,

$$A = C + A_0 \cdot e^{-x/\Delta\nu}. \tag{7}$$

In a model with a single thin scattering screen, the angular size of the scattering disk is related to the scattering time scale and the distance to the screen by the expression [25]:

$$\theta^2 = \frac{8c\tau\ln 2(1-\alpha)}{\alpha L}, \tag{8}$$

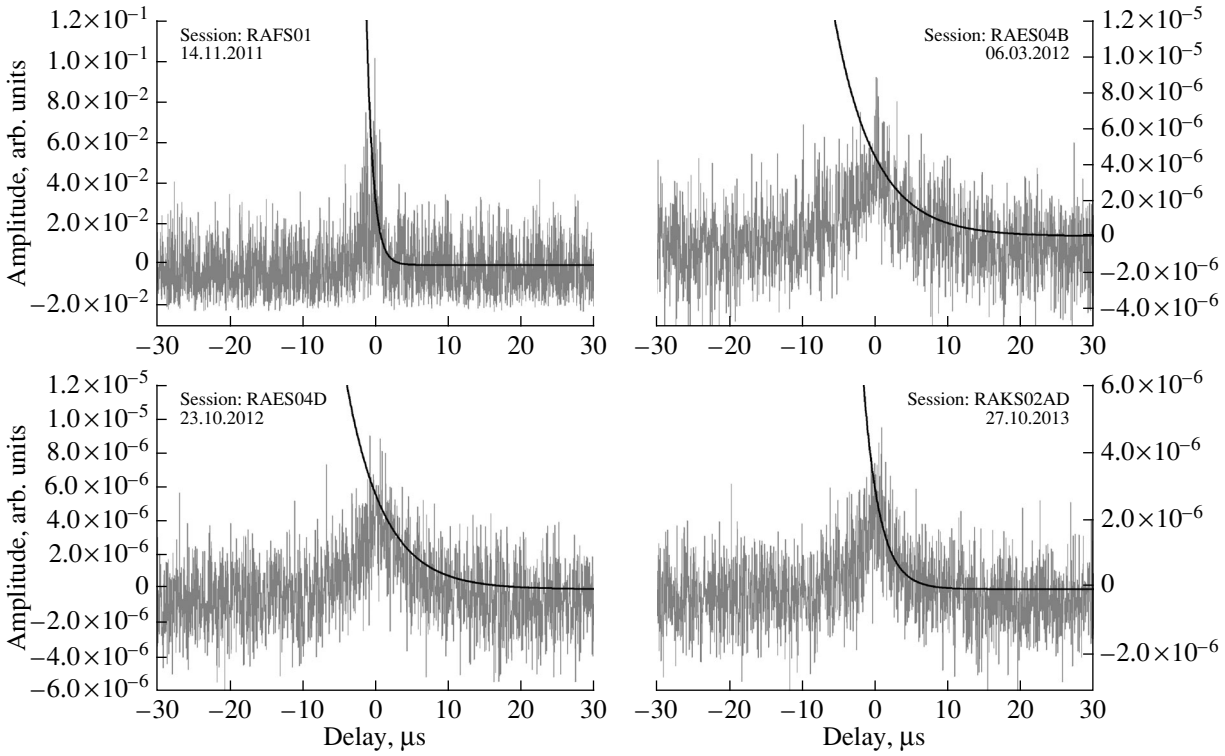

Fig. 5. Averaged visibility amplitudes for the ground–space baselines between RadioAstron and the most sensitive ground telescope. The sessions took place on November 14, .2011, March 6, 2012, October 23, 2012, and October 27, 2013 (from left to right, top to bottom). The solid curves show the exponential fits used to estimate the scattering time scale.

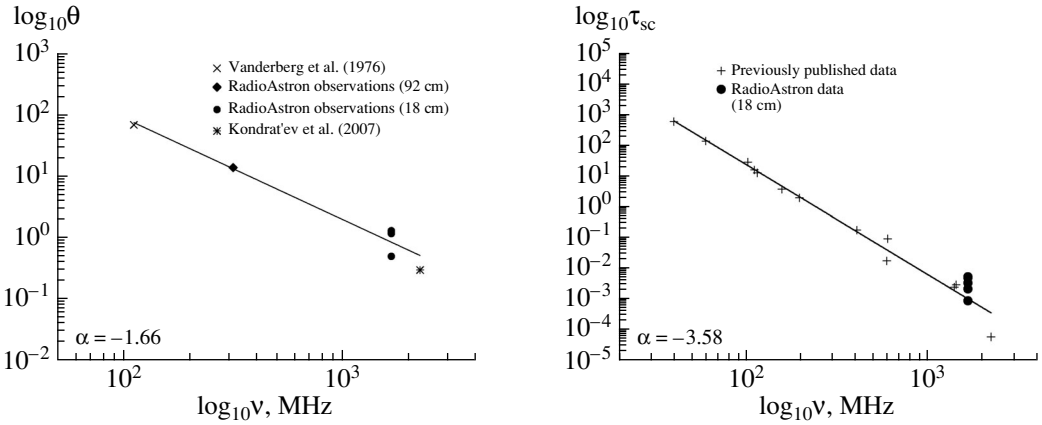

Fig. 6. Frequency dependence of the angular size of the scattering disk (left) and the scattering time scale (right) on a logarithmic scale. The lines correspond to power-law dependences with the index $\alpha = -1.66$ for the frequency dependence of the scattering disk and $\alpha = -3.58$ for the frequency dependence of the scattering time scale.

where $L = 2$ kpc is the distance to the Crab pulsar, $\alpha = D/L$ the distance from the observer to the scattering screen divided by L, τ the scattering time scale, and c the speed of light.

Knowing the angular size of the scattering disk θ and the scattering time scale τ, we can determine the relative distance to the scattering screen α:

$$\alpha = \frac{8c\tau \ln 2}{\theta^2 L + 8c\tau \ln 2}. \quad (9)$$

Our estimates of the angular size of the scattering disk and the scattering time scale are in good agreement with previously published results (Fig. 6). Our results confirm the power-law dependence with

Table 2. Measured scattering parameters

Session	τ_{SC} (μs)	θ (mas)	$\Delta\nu$ (kHz)	R_{diff} (km)	α	Number of GPs
RAFS01	0.9 ± 0.1	1.3 ± 0.2	116.3 ± 24.5	$10\,361 \pm 1700$	0.36 ± 0.08	98
RAES04A	5.8 ± 0.3	0.6 ± 0.1	55.2 ± 5.9	$21\,817 \pm 2900$	0.94 ± 0.02	1202
RAES04B	5.5 ± 0.7	0.5 ± 0.1	41.2 ± 7.9	$26\,949 \pm 7700$	0.96 ± 0.03	1034
RAES04D	5.1 ± 0.5	1.2 ± 0.1	40.7 ± 4.6	$11\,413 \pm 900$	0.79 ± 0.03	929
RAKS02AD	2.2 ± 0.3	1.2 ± 0.1	78.1 ± 7.9	$12\,113 \pm 1200$	0.61 ± 0.06	453
RAKS02AE	–	14.0 ± 1.4	–	5140 ± 500	–	579

index $\alpha = -1.66$ for the frequency dependence of the angular size of the scattering disk and with index $\alpha = -3.58$ for the frequency dependence of the scattering time scale.

5. CONCLUSION

We have obtained interferometric fringes for giant pulses of the Crab pulsar on ground–space baselines extending to 150 000 km for the first time, in VLBI observations with the RadioAstron space radio telescope.

We have detected a transformation of the shape of the visibility function of the giant pulses in the transition from ground to ground–space baselines exceeding the radius of the diffraction spot (Fig. 4). The visibilty amplitude for the ground baselines is dominated by a narrow feature, which is absent in the visibility amplitudes for the ground–space baselines, and the shape of the cross-correlation function is fairly broad, and consists of numerous peaks.

Table 2 presents all the parameters for which we have obtained estimates. The angular size of the scattering disk was estimated assuming a uniform scattering disk (points for the ground–space baselines were not included) and for each observing session. Figure 3 shows the resulting dependence of the visibility amplitudes on the projected baseline, where the curves depict fits using the relation (4).

Despite the absence of fringes on long projected baselines (>40 000 km), when the scattering disk is resolved, the correlated visibilities have appreciable amplitudes that differ from zero. Moreover, the visibility amplitude remains essentially constant as the projected baseline length is further increased to 150 000 km. This fact, together with the observed variation of the shape of the visibility amplitudes on such projected baselines, provides evidence that the ground–space baselines are resolving inhomogeneities present in the scattering disk. This effect has also been observed for the pulsar B0329+54 [24].

The distribution of the visibility function with the projected baselines is consistent with the theory of Goodman and Narayan [26].

Earlier studies already indicated the presence of two scattering components, one located close to the Crab Nebula and another constant component due to the interstellar plasma [27–29]. In particular, Karuppusamy et al. [30] showed the presence of variations of the scattering of the Crab pulsar during six observing sessions, and demonstrated that the dominant region of scattering was located in the vicinity of the Crab Nebula.

In our case, the distance to the scattering screen was found to have different values for each session. In the first session (RAFS01), the distance to the screen corresponds to the case of approximately equally distributed scattering material along the line of sight $d = D/3$ [31]. In other sessions, scattering in the vicinity of the Crab Nebula was dominant. The variation of the parameter α from session to session indicates the need to use a model with several scattering screens in future analyses of such data.

ACKNOWLEDGMENTS

We thank T.V. Smirnova of the Pushchino Radio Astronomy Observatory for valuable help and comments on this work. We also thank Carl Gwinn and Michael Johnson for their contribution to the preparation of the scientific proposals and valuable discussions of these results.

The RadioAstron project has been realized by the Astro Space Center, the Lebedev Physical Institute, Russian Academy of Sciences and the S.A. Lavochkin Scientific Production Association under contract to the Russian Space Agency, jointly with many scientific and technical organizations in Russia and other countries.

The results presented here have been based partially on observations carried out on radio telescopes of the Institute of Applied Astronomy of the Russian Academy of Sciences.

These studies have been based partially on observations carried out on the 70-m Evpatoria radio telescope (Ukraine) by the Radio Astronomical Institute of the National Academy of Sciences of the Ukraine, under contract to the State Space Agency of the Ukraine and the National Center for the Management and Testing of Space Resources, with technical support from the Astro Space Center, Lebedev Physical Institute, Russian Academy of Sciences.

These studies have been based partially on observations with the European VLBI Network.

This work was supported by the Russian Foundation for Basic Research (grant 13-02-00460).

REFERENCES

1. P. A. G. Scheuer, Nature **218**, 920 (1968).
2. B. J. Rickett, Ann. Rev. Astron. Astrophys. **15**, 479 (1977).
3. J. W. Armstrong, B. J. Rickett, and S. R. Spangler, Astrophys. J. **443**, 209 (1995).
4. V. I. Shishov and T. V. Smirnova, Astron. Rep. **46**, 731 (2002).
5. V. I. Shishov, T. V. Smirnova, W. Sieber, V. M. Malofeev, V. A. Potapov, D. Stinebring, M. Kramer, A. Jessner, and R. Wielebinski, Astron. Astrophys. **404**, 557 (2003).
6. T. V. Smirnova, C. R. Gwinn, and V. I. Shishov, Astron. Astrophys. **453**, 601 (2006).
7. T. V. Smirnova, V. I. Shishov, M. V. Popov, C. R. Gwinn, J. M. Anderson, A. S. Andrianov, N. Bartel, A. Deller, M. D. Johnson, B. C. Joshi, N. S. Kardashev, R. Karuppusamy, Y. Y. Kovalev, M. Kramer, V. A. Soglasnov et al., Astrophys. J. **786**, 115 (2014).
8. V. I. Shishov, Astron. Rep. **37**, 378 (1993).
9. T. H. Hankins, J. S. Kern, J. C. Weatherall, and J. A. Eilek, Nature **422**, 141 (2003).
10. M. V. Popov, V. A. Soglasnov, V. I. Kondratiev, A. V. Bilous, S. V. Sazankov, A. I. Smirnov, B. Z. Kanevskii, V. V. Oreshko, and Yu. P. Il'yasov, Astron. Rep. **52**, 900 (2008).
11. A. Jessner, M. V. Popov, V. I. Kondratiev, Y. Y. Kovalev, D. Graham, A. Zensus, V. A. Soglasnov, A. V. Bilous, and O. A. Moshkina, Astron. Astrophys. **524**, A60 (2010).
12. M. V. Popov, V. A. Soglasnov, V. I. Kondratiev, S. V. Kostyuk, Yu. P. Il'yasov, and V. V. Oreshko, Astron. Rep. **50**, 55 (2006).
13. V. I. Kondratiev, M. V. Popov, V. A. Soglasnov, Y. Y. Kovalev, N. Bartel, W. Cannon, and A. Y. Novikov, Astron. Astrophys. Trans. **26**, 585 (2007).
14. N. S. Kardashev, V. V. Khartov, V. V. Abramov, V. Yu. Avdeev, A. V. Alakoz, Yu. A. Aleksandrov, S. Ananthakrishnan, V. V. Andreyanov, A. S. Andrianov, N. M. Antonov, M. I. Artyukhov, M. Yu. Arkhipov, W. Baan, N. G. Babakin, N. Bartel, et al., Astron. Rep. **57**, 154 (2013).
15. A. S. Andrianov, I. A. Girin, V. E. Zharov, V. I. Kostenko, S. F. Likhachev, and M. V. Shatskaya, Vestn. NPO Lavochkina **3**, 55 (2014).
16. R. N. Manchester, G. B. Hobbs, A. Teoh, and M. Hobbs, Astrophys. J. **129**, 1993 (2005).
17. A. G. Lyne, R. S. Pritchard, and F. Graham-Smith, Mon. Not. R. Astron. Soc. **265**, 1003 (1993).
18. G. B. Hobbs, R. T. Edwards, and R. N. Manchester, Mon. Not. R. Astron. Soc. **369**, 655 (2006).
19. J. M. Wrobel and R. C. Walker, ASP Conf. Ser. **180**, 171 (1999).
20. C. R. Gwinn, M. C. Britton, J. E. Reynolds, D. L. Jauncey, E. A. King, P. M. McCulloch, J. E. J. Lovell, and R. A. Preston, Astrophys. J. **505**, 928 (1998).
21. C. R. Gwinn, N. Bartel, and J. M. Cordes, Astrophys. J. **410**, 673 (1993).
22. V. I. Shishov, Sov. Astron. **17**, 598 (1973).
23. I. P. Williamson, Mon. Not. R. Astron. Soc. **166**, 499 (1974).
24. M. V. Popov, A. S. Andrianov, N. Bartel, C. R. Gwinn, M. D. Johnson, B. C. Joshi, N. S. Kardashev, R. Karuppusamy, Y. Y. Kovalev, M. Kramer, A. G. Rudnitskii, E. R. Safutdinov, V. I. Shishov, T. V. Smirnova, V. A. Soglasnov et al., Astrophys. J. (in press).
25. M. C. Britton, C. R. Gwinn, and M. J. Ojeda, Astrophys. J. **501**, L101 (1998).
26. J. Goodman and R. Narayan, Mon. Not. R. Astron. Soc. **238**, 963 (1989).
27. C. C. Counselman III and J. M. Rankin, Astrophys. J. **166**, 513 (1971).
28. J. M. Rankin and C. C. Counselman III, Astrophys. J. **181**, 875 (1973).
29. A. G. Lyne and D. J. Thorne, Mon. Not. R. Astron. Soc. **172**, 97 (1975).
30. R. Karuppusamy, B. W. Stappers, and W. van Straten, Astron. Astrophys. **515**, A36 (2010).
31. K. M. Desai, C. R. Gwinn, J. Reynolds, E. A. King, D. Jauncey, C. Flanagan, G. Nicolson, R. A. Preston, and D. L. Jones, Astrophys. J. **393**, L75 (1992).

Translated by D. Gabuzda